Science and Technology Indonesia
e-ISSN:2580-4391 *p*-ISSN:2580-4405
Vol. 9, No. 4, October 2024

Research Paper

Carbon Micron-size Content Dependency in Epoxy/Carbon Composite Coated onto SPCC Plate for Automotive Bodies Protection

Rani Anggrainy[1*], Ferry Budhi Susetyo[1], Ahmad Lubi[1], Sigit Dwi Yudanto[2], Cahaya Rosyidan[3], Bambang Soegijono[4], Maman Kartaman Ajiriyanto[5], Ova Kurniawan[6], Dwi Nanto[7]

[1]*Department of Mechanical Engineering, Universitas Negeri Jakarta, Jakarta Timur, DKI Jakarta, 13220, Indonesia*
[2] *Research Center for Metallurgy-National Research and Innovation Agency, Tangerang Selatan, Banten, 15314, Indonesia*
[3]*Department of Petroleum Engineering, Universitas Trisakti, Jakarta Barat, DKI Jakarta 11440, Indonesia*
[4]*PROUDTEK Lab., Department of Geosciences, Universitas Indonesia, Depok, Jawa Barat, 16424, Indonesia*
[5]*Research Center for Nuclear Material and Radioactive Waste Technology, National Research and Innovation Agency, Tangerang Selatan, Banten, 15314, Indonesia*
[6]*Department of Electrical Engineering, Institut Teknologi PLN, Jakarta Barat, DKI Jakarta, 11750, Indonesia*
[7]*Department of Physic Education, UIN Syarif Hidayatullah, Jakarta, 15412, Indonesia*
***Corresponding author**: rani_anggrainy@unj.ac.id

Abstract
Conventional epoxy coating for surface metal corrosion protection reported many unsolved technical problems. Adding filler in the epoxy could enhance the promising properties of the composite coating. Our work describes in detail the synthesizing and characterizing epoxy/carbon composite coating. Epoxy was mixed with thinner high gloss (HG) and hardener and stirred using a stirrer apparatus. After blending, various carbons were added (1 wt. %, 3 wt. %, and 5 wt. %) and then appropriately stirred. The different mixture composite was coated onto the steel plate cold rolled coiled (SPCC) plate using high-volume low-pressure (HVLP) in two passes. Various characterizations were performed, including crystallographic orientation, Infra-Red (IR)-spectra, surface morphology, thickness, hydrophobicity, hardness, and corrosion using X-ray diffraction (XRD), Fourier transform infrared (FTIR), Scanning electron microscopy (SEM), portable dry film coating thickness (DFT), digital camera, Vickers microhardness tester, and Potentiostat, respectively. More carbon micron-sized content led to elevate the peak intensity, surface bumpiness, and hydrophobicity. The uppermost external bumpiness and hydrophobicity values are 23.51 μm and 101°. Hardness depends on carbon content and more carbon leads to an increase in the hardness of the composited coating. The highest average Vickers hardness value is 28.24 HV. The coating thickness influenced the corrosion rate, more coating thickness promoted lesser corrosion rate. The highest coating thickness (60.8 μm) promoted a corrosion rate of around 5.65×10^{-4} mmpy.

Keywords
Crystallographic Orientation, IR-Spectra, Film Properties, Hardness, Corrosion

Received: 23 June 2024, Accepted: 5 September 2024
https://doi.org/10.26554/sti.2024.9.4.989-998

1. INTRODUCTION

Protective coating for automotive bodies uses epoxy due to its excellent chemical resistance, better corrosion resistance, and superior electrical resistivity (Merneedi et al., 2021; Sakib and Iqbal, 2021). Therefore, coating in automobiles uses epoxy as a primer coat. A primer coat applied intents to improve adhesion between the urethane or poly vinyl carbon (PVC) and metallic base. Besides that, it provides more corrosion protection and increases the paint's appearance (Jin et al., 2015). The primer coating could also fill minor imperfections and scratches caused during surface preparation (Akafuah et al., 2016). Xia et al. (2014) coating bare Q235 steel using epoxy and then immersing it in seawater (100 hours), found a decrease in corrosion current density from 7.54 to 0.0948 μA/cm^2. However, the epoxy coating has several limitations, such as lower hardness, toughness, and impact resistance. Consequently, accumulating filler to the epoxy could enhance the condition of the composite coating.

Several fillers, such as carbon, clay, and silicon (Si), were added to epoxy coatings, which attracted considerable attention in the academic and industrial fields (Al-Zu'bi et al., 2023; Deyab et al., 2018). Mateab and Albozahid (2022) found that increased carbon lead increases the composite hardness. Salam et al. (2016) introduced clay in epoxy, and increasing clay content leads to decreased hardness and flexural strength. Ma et al.

(2024) modified Si through a plasma interface in a nitrogen atmosphere. Then, they added modified Si and unmodified Si separately in epoxy, resulting in a composite coating with modified Si that successfully enhanced the hardness and corrosion resistance.

Carbon has superior properties such as higher hardness; therefore, adding carbon to the epoxy could enhance the composite properties (Duleba et al., 2015; Wang et al., 2015). Besides that, presenting carbon in epoxy coating also could enhance the corrosion property. Li et al. (2022) has stated presenting 0.15 wt.% of N-doped carbon nanodots (CNDs) in the epoxy could advance anti-corrosion of the coating than pure epoxy coating. Merneedi et al. (2021) added carbon nanotube (1%, 2%, 3%, and 4%) into epoxy resulting an increase in hardness and tensile strength within increased carbon nanotube content. Qu et al. (2020) added carbon fiber micron-size (0.05%, 0.1%, 0.2%, 0.35%, and 0.5%) into epoxy resulting in an increase in flexural strength within increased carbon content from 0 to 0.2%. On the contrary, more carbon content (0.35% and 0.5%) tends to decrease flexural strength. Sheth et al. (2020) added a carbon nanotube (0.5%, 1.0%, 2.0%, and 2.5%) into epoxy resulting in a growth in tensile and flexural strong point with a growth in carbon content from 0 to 1.0%. On the contrary, more carbon nanotube content (1.5% and 2.0%) tends to decrease tensile and flexural strength. Weng et al. (2024) added carbon fiber to epoxy with ratio 15:85, 20:80, 25:75, 30:30, and 35:65 resulting increase in the thermal conductivity, and stress within increase in carbon content. The influence of multi-wall carbon nanotubes (MWCNT) and few layered graphene (FLG) in carbon fiber reinforced epoxy (CFRP)/epoxy have been investigated by Knoll et al. (2014) Tensile strength and Young's modulus could be enhanced by presenting 0.3 wt.% MWCNT in the CFRP/epoxy. Khun et al. (2014) in their study, adding MWCNT with concentration of 0.1 wt.% and 0.5 wt.%, resulting in an increased MWCNT lead to increase in adhesion strength, wear resistance, corrosion resistance. Basha et al. (2022) has coated concrete with mixing epoxy with various submicron/nano-carbon (0%, 0.25%, 0.5%, 0.75%, and 1%) resulting increase in submicron/nano-carbon content lead to increase coating adhesion and compressive strength.

As mentioned above, various investigations are being conducted for carbon addition in epoxy composite coating. However, the discussion is not yet comprehensive for carbon micro-size addition. Therefore, further studies about the epoxy-carbon coating are needed, especially for composite coating characterization. In this research, various filler concentrations were added to the epoxy coating. This research was adopted from a previous study (Kurniawan and Soegijono, 2020), which added 5 wt.% of carbon into Polyurethane coating. Moreover, several researchers focused on carbon content < 1 wt. % (Khun et al., 2014; Knoll et al., 2014; Li et al., 2022). Therefore, the present study varies carbon 1 wt.%, 3 wt.%, and 5wt.%. Several observations were conducted, including crystallographic orientation, Infra-Red (IR)-spectra, surface morphology, thickness, hydrophobicity, hardness, and corrosion. Adding a micro-size filler in epoxy, as expected, could improve the composite coating properties.

2. EXPERIMENTAL SECTION

2.1 Materials

Commercial product (industrial grade) produces bisphenol A diglycidyl ether (BADGE) type epoxy and hardener. Carbon type as a filler was used in the present research, similar to the previous study (Kurniawan and Soegijono, 2020). SPCC plate (200 mm × 200 mm × 1 mm) was used as substrate with composition 0.125 wt.% C, 0.185 wt.% Mn, 0.022 wt.%, 0.018 wt.% P, 0.013 wt.% S and Fe balance.

2.2 Synthesis of Composite Coating

Epoxy was mixed with thinner high gloss (HG) and hardener with composition 0.8 L : 0.5 L : 0.2 L (8 : 5 : 2), then stirred using a stirrer apparatus. After blending, various carbons were added (1 wt.%, 3 wt.%, and 5 wt.%) and then appropriately stirred. The sample was designated EC1, EC3, and EC5 for 1 wt.%, 3 wt.%, and 5 wt.% of carbon addition, respectively. The present research focuses on carbon dependency, therefore epoxy without carbon was not investigated (Merneedi et al., 2021). A few parts of the mixture composite coating were dried at room temperature (one week) for investigations of X-ray diffraction (XRD) and Fourier transform infrared (FTIR).

2.3 Sample Preparation

After the mixture composite was ready to coat onto the steel plate cold rolled coiled (SPCC) plate, severe surface preparations should be conducted. SPCC plates were cleaned using a wire brush; then cleaned using thinner and dried before the coating was applied. Afterward, the mixture composite coating was applied onto the SPCC plate using an HVLP conventional spray gun with a nozzle tip hole size of 0.6 mm and air pressure of 6 kg/cm^2 (Two coating passes were applied). Coated samples were dried in air at room temperature (one week) and then cut for further characterization such as Scanning electron microscopy (SEM), hydrophobicity, hardness, and corrosion test.

2.4 Characterization

XRD measurement using PANalytical (CuK radiation) was performed. XRD investigations were scanned from 5° to 90° using step size 0.0217°. Collected data was refined using Highscore software plus it was used for crystallographic orientation. Moreover, FTIR using Bruker: Alpha from 400-4000 cm^{-1} was performed. Afterward, SEM was investigated using FE-SEM FEI (Quanta 650) at 1000 magnification. MATLAB software was used for uneven surface investigations based on SEM images. The uneven surface parameters such as average, and standard deviation, were found using the statistical analysis using MATHLAB. Firstly, the SEM image was converted to histogram, then changed into grey scale followed by analysis of the grey scale. Secondly, resulting 3D plot surface, counting

average of the array, followed by counting standard deviations and average using statistical analysis. The coefficient variant (CV) of coating surfaces, using Equation (1), can be calculated (Rwawiire et al., 2014).

$$CV\% = \frac{\text{Standard Deviation}}{\text{Average}} \times 100 \quad (1)$$

Moreover, surface roughness was investigated using image-J software through image processing based on SEM pictures. Roughness is defined as the degree of smoothness of form that appears because of the production or synthesis process. The amount of roughness is measured using the average roughness value (Ra). Ra is defined as the arithmetic mean value of the deviation of the roughness profile from the average center line. The relationship between distance (μm) and the grey value of the surface of each sample shows that the grey value fluctuates as the distance (μm) increases.

The AMTAS-AMT15 portable dry film coating thickness (DFT) apparatus was used to measure the coating thickness. Before measurement, the portable DFT was calibrated using a sheet standard from the manufacturer. The coating thickness on the uppermost surface of the sample was measured after it was dried at room temperature for one week in air. The spot of the test film thickness is presented in Figure 1.

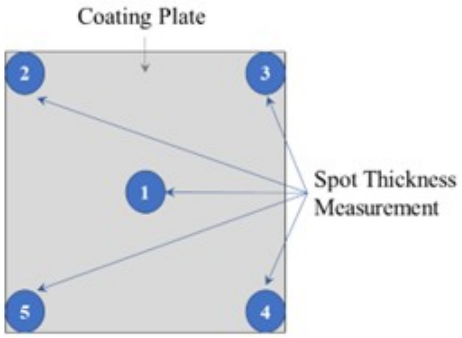

Figure 1. Spot Film Thickness

A water droplet was put on top of the composite coating, and a digital camera was used to document. Afterward, hydrophobicity measurements were conducted by measuring the contact perspective of the water droplets on the outward composite coating. Hydrophobicity criteria were investigated according to the angle formed and compared to previous research (Kurniawan and Soegijono, 2020).

The hardness test was conducted based on the ASTM E384 standard. The present study used a Vickers microhardness tester apparatus with 30 g of load (15 sec of dwell time). The hardness test was performed on the top surface of the coated sample. Hardness test measurement was conducted of three repeatable measurements.

A Potentiostat (Digi-Ivy DY 2300 series) performed a corrosion test measurement at room temperature. Platinum, Ag/AgCl, and composite coating (1 cm^2) were subjected as counter, reference, and working electrodes. At room temperature, measurement was performed at 50 mV/s of scan rate in 3.5% sodium chloride solution. Finally, the corrosion rate was calculated using the following equation (Susetyo et al., 2021).

$$CR\ (mmpy) = C\frac{I_{corr} \times M}{\rho \times n} \quad (2)$$

Where I_{corr} is corrosion current density (A/cm^2), C is corrosion constant (3.27 mmpy), whereas M is the atomic weight (g/mol), is density (g/cm^3), and n is number electron involved.

3. RESULT AND DISCUSSION

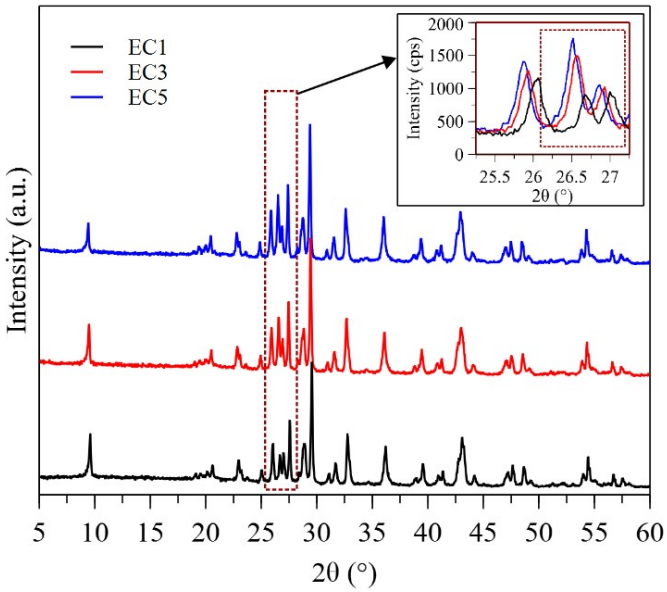

Figure 2. XRD Patterns of Composite Coating. The Inset Image Shows the Magnification Patterns at 2θ=25.25 – 27.25°

3.1 XRD

The diffraction patterns of the samples EC1, EC3, and EC5 have been depicted in Figure 2. In all samples, there is a tendency towards a crystalline structure. Adding carbon to epoxy resin results in a carbon-epoxy composite with a crystalline structure, as reported by Hassan et al. (2020). Using XRD data, it is possible to identify that the epoxy resin-carbon composite has a crystalline structure, as evidenced by the identical diffraction patterns in all three samples. However, one of the peaks with a diffraction pattern magnification angle of 2θ = 25.25°–27.25° also exhibits an increase in intensity (see inset image in Figure 2). The carbon peak arises at 2θ = 26.57° (Kurniawan and Soegijono, 2020), where the intensity increases in the samples. Thus, the level of carbon concentration causes an intensification in the peak intensity of the carbon phase.

3.2 FTIR

The FTIR is a reliable and simple method to examine organic and inorganic compounds related to functional groups (Bibi

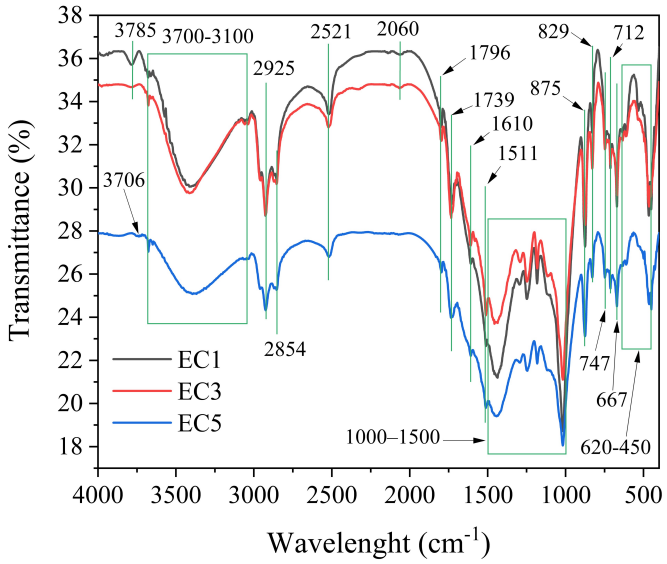

Figure 3. FTIR Spectra of Various Composite Coating

et al., 2022). Epoxy has a hydrophilic chemical group such as a hydroxyl group (OH), a carboxyl group (C=O), and an amino group (NH_2). FTIR spectra of various coatings are presented in Figure 3.

According to Figure 3, several bands are seen, which indicate certain functional groups. O−H stretching vibration in hydroxyl (−OH) and carboxyl (−COOH) is seen at wavelength 3785 cm^{-1} and 3706 cm^{-1} (Bibi et al., 2022). 3700-3100 cm^{-1} band representation of vibrating of O−H and C=O probably due to curing reaction of epoxy/carbon (Netkueakul et al., 2020). A band at 2925 cm^{-1} is assigned to C−H stretch vibration (Asemani and Rabbani, 2020). CH_2 symmetric stretching was found at wavelength 2854 cm^{-1} (Sudha et al., 2017). A band at 2521 cm^{-1} is represented as out-of-plane vibration of O−H (Qi et al., 2017). Wavelength at 2060 cm^{-1} is attributed to C=O bending vibration stretching (Zhang et al., 2022). The peaks at 1739 cm^{-1} and 1796 cm^{-1} attributed to C=O stretching mode was present as antisymmetric and symmetric (Bouhamed et al., 2018). The aromatic rings are attributed to 1610 and 1511 cm^{-1} bands (Soares-Pozzi and Dibbern-Brunelli, 2016). Bands at 1000-1500 cm^{-1} attributed to S=O group (Freshtegan et al., 2016). The band at 875 cm^{-1} is attributed to absorbing signals of benzene ring (Liang et al., 2017). A peak at 829 cm^{-1} represents C−H out of plane deformation (Zuo et al., 2019). 747 cm^{-1} N−H band wagging vibration (Eskizeybek et al., 2017). 712 cm^{-1} band associated with a carbonyl-hydroxyl H bond (Mora et al., 2020). 667 cm^{-1} is qualified to stretching vibration of the C−Cl bond (Xu et al., 2020). Bands at 620-450 cm^{-1} attributed to the residual of the catalyst (Maron et al., 2018). In conclusion, the carbon content increased from 3 to 5 wt.% led to a shifted band from 3785 to 3706 cm^{-1}, which indicated the transformation of O−H stretching vibration in −OH to be O−H stretching vibration in −COOH. Carbon content increased from 3 to 5 wt.% also led to almost disappearing peak of 2060 cm^{-1} probably break transformation of C=O to be C−O. Generally, it can be concluded that carbon/epoxy composite coating was successfully synthesized.

3.3 SEM, Uneven, and Roughness

SEM of various coatings at a magnification of 1000× is depicted in Figure 4. All samples show a homogeneous topographic distribution. Several coating defects, such as blisters and blushing, are not seen on the surface. Commonly, a blister occurs due to air bubble formation on the painted specimen. Moreover, blushing defects are due to inappropriate humidity, and then a white cloud forms on the specimens (Almansoori et al., 2021). It can be concluded that carbon-epoxy forms a perfect agglomeration and could be applied using the HVLP spray apparatus. Furthermore, uneven surface morphology is presented in all the coatings. Therefore, MATHLAB analysis is used to profoundly explore the inconsistent trend of surface morphology, as seen in Figure 5.

The statistical analysis, such as average, standard deviation, and CV value based on MATHLAB investigation, can be seen in Table 1. CV can be found by inserting the average and standard deviation into Equation (1). CV values indicate the unevenness of the coating surfaces. Higher CV values indicate a more uneven surface morphology of the coating. According to Table 1, an increase in the carbon content in the composite layer led to an uneven rise in the surface. This result means the carbon concentration influences the unevenness of the coating surface in the composited coating.

Table 1. Matlab Statistical Analysis Result

Coating	Average	Standard Deviation	CV (%)
EC1	99.70	37.77	37.89
EC3	96.98	36.75	37.90
EC5	97.79	38.07	38.93

Deep explorations about the surface of the coating using image-J software are needed. Therefore, the present study investigated roughness analysis of the surface-coated samples using image-J software. The result of the surface roughness analysis is presented in Figure 6. According to Figure 6, the surface roughness (Ra) of the EC1, EC3, and EC5 samples are 22.17 μm, 23.14 μm, and 23.51 μm, respectively. Chen et. al. have found that the present MWNCTs (0.2%) in the epoxy lead to an increase in surface roughness from 0.93 to 1.17 nm (Chen et al., 2021). Thus, the condition indicates that the carbon inserted in the epoxy could influence the roughness of the surface.

The size of the carbon that was inserted also affected the surface roughness. In intensification in exterior roughness is caused by the higher dimension of the carbon led to. Moreover, the carbon content in the composite coating also influences the roughness. Based on the image-J software analysis result in

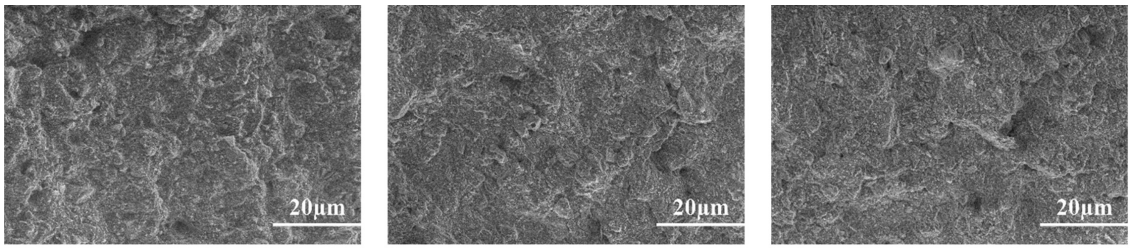

Figure 4. SEM of Various Composite Coating

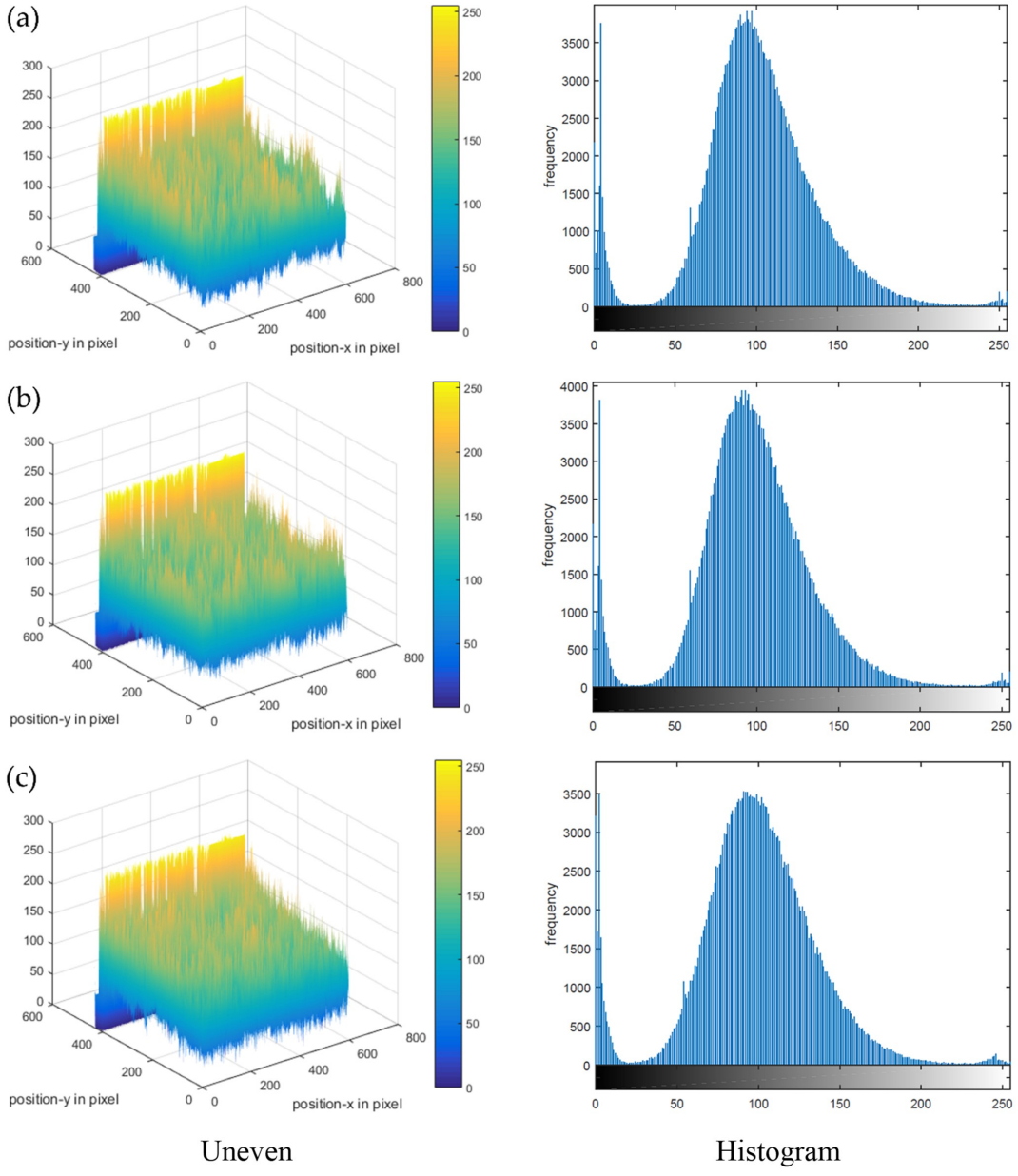

Figure 5. Uneven Surface of Various Composite Coating

the present result, it can be concluded that increased carbon content increases surface roughness.

3.4 Composite Coating Thickness

A dry film thickness (DFT) apparatus was used to measure the various coated samples to get the coating thickness. The

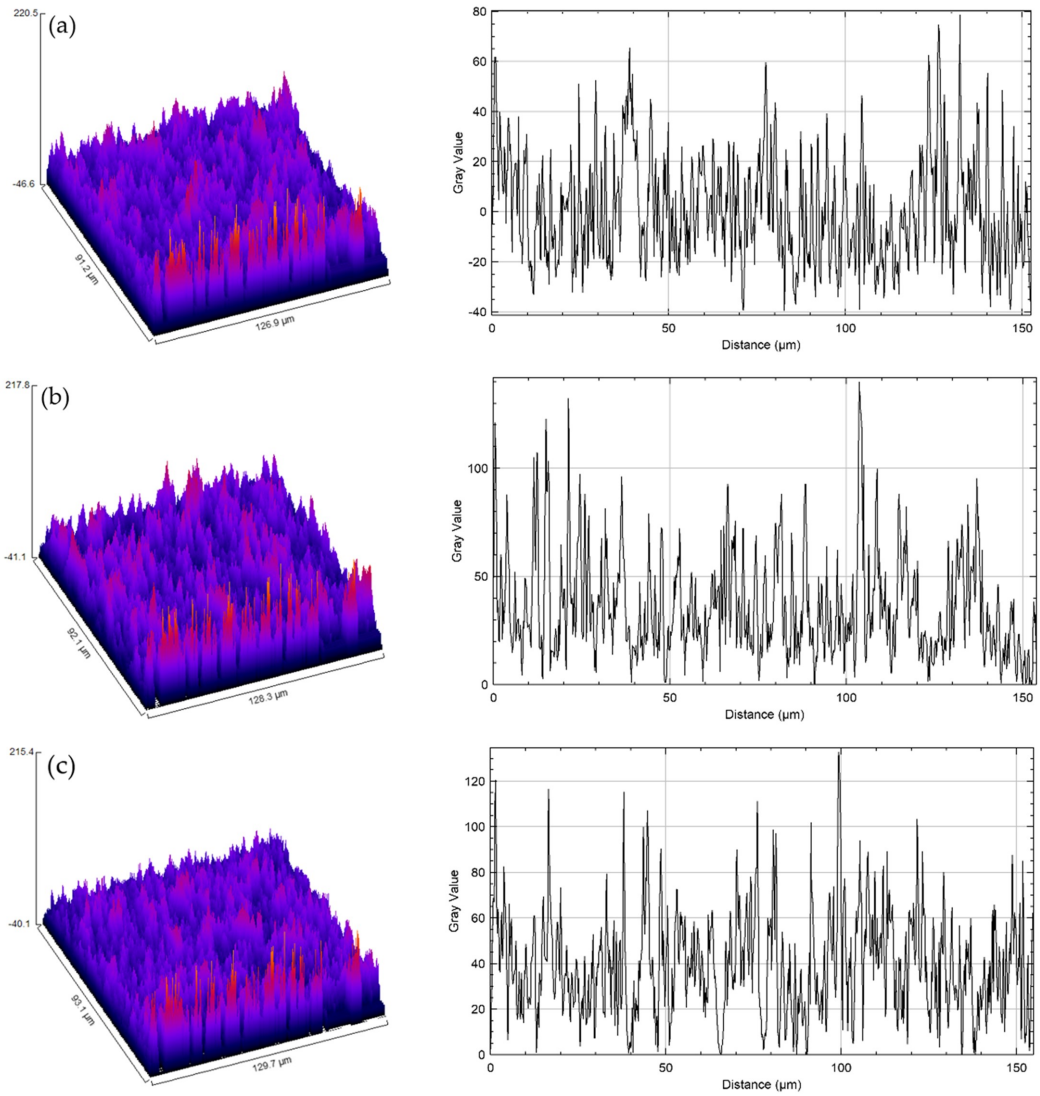

Figure 6. Surface Roughness of Various Composite Coating

measurement result of all samples is depicted in Figure 7. The external surfaces of an automobile body need a thickness of around 30-40 μm of coating for a primer to reach chipping protection and increase the paint's appearance (Akafuah et al., 2016). Moreover, each coating layer is commonly in the range of 10-100 μm layered on top of each other (Vaßen et al., 2019). Figure 7 shows that layer thickness varies between 57.4 to 60.8 μm. The EC3 sample has a lower thickness than others; inversely, the EC5 sample has a higher thickness. Based on the experimental experiences, it wasn't easy to reach a similar thickness of three samples due to conventional HVLP being used in this experiment; hence, it was difficult to control (Almansoori et al., 2021).

Moreover, several factors that influence the DFT are spray pressure, nozzle size, and spray time. Higher spray pressure decreases DFT due to a lack of spreading momentum and stability, which results in smaller droplets. Longer spray durations and higher nozzle sizes result in more DFT due to more material consumption in the painting process, forming thicker coatings (Luangkularb et al., 2014).

3.5 Hydrophobicity Test

The water contact angle is an important parameter in finding the wettability of the composited coating. A small contact angle means easily spreading the droplets on the coating surface. This condition means increased wettability of the layer. According to Figure 8, in the water contact angle rise due to evidently increase in the carbon. The water contact angle can increase due to increased surface roughness with increased carbon con-

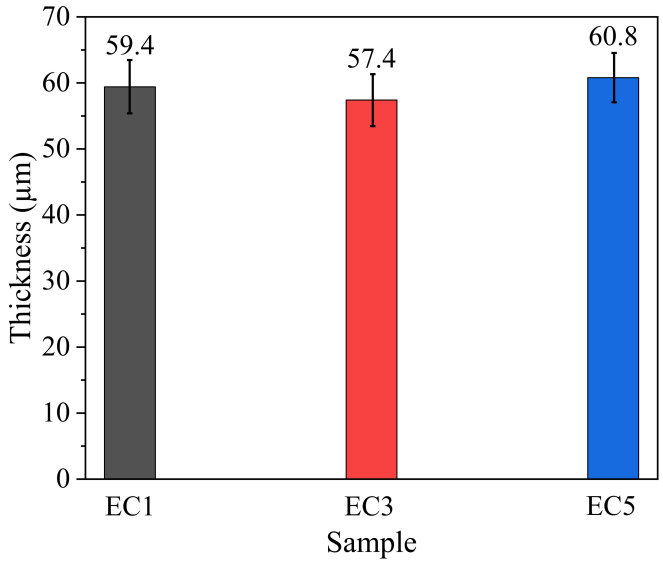

Figure 7. Film Thickness of Various Composites Coating

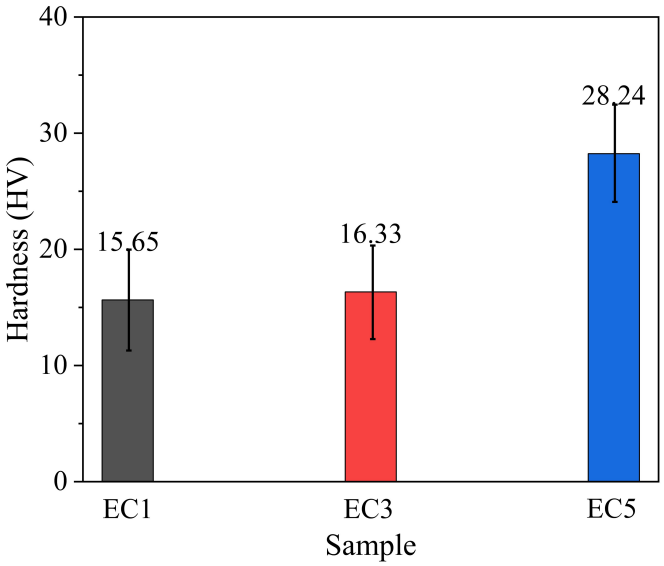

Figure 9. Hardness Test Results of Various Composite Coating

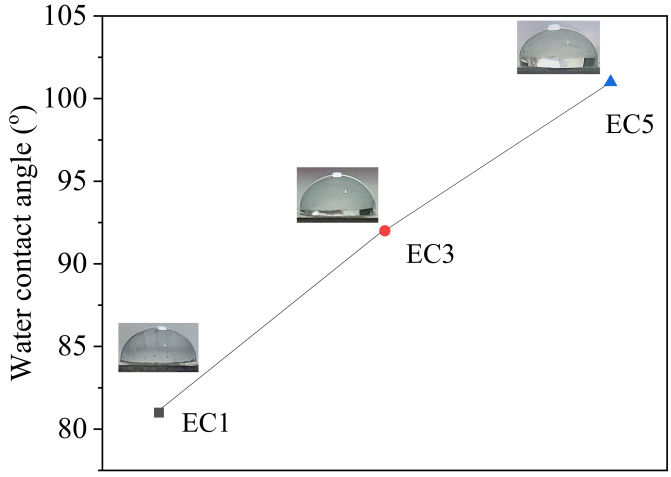

Figure 8. Hydrophobicity Test Results of Various Composite Coating

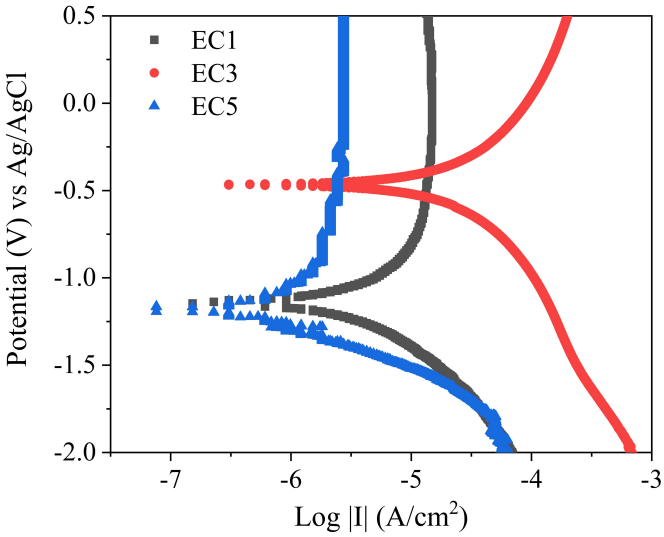

Figure 10. Corrosion Test Results of Various Composite Coating

tent, which perfectly agrees with result in Table 1. According to Cheng et al. (2023)'s report, increased surface roughness promoted a higher water contact angle . Moreover, Edvardsen et al. (2021) found that pure epoxy has 61°, and epoxy/carbon nanofiber coating around 72° of contact angle. Compared with the present research, Edvardsen et al. (2021) has less water contact angle, probably due to the carbon nano size used in the study. Consequently, less roughness and promoted to resulting less water contact angle. According to Kurniawan and Soegijono (2020), the water contact angle between $90° \leq \theta < 150$ is hydrophobic and $90° < \theta$ criteria. Cured epoxy has a hydrophilic chemical group such as a hydroxyl group (OH), a carboxyl group (C=O), and an amino group (NH_2); therefore, epoxy has 49°-61° of water contact angle (Edvardsen et al., 2021). Moreover, according to Figure 8, EC1, EC3, and EC5 samples have water contact angles of 81°, 92°, and 101° (respectively). Therefore, samples EC3 and EC5 are hydrophobic, and sample EC1 is hydrophilic. The result indicates the change from hydrophilic to hydrophobic by the addition of carbon, and the wettability of the coating surface is lower at higher carbon content. A sample with hydrophobic criteria tends the droplet to have more difficulty spreading on the coating surface, which means decreased wettability of the layer.

3.6 Hardness Test

A hardness apparatus was used to measure the various coated samples to get the coating hardness values. The hardness mea-

surement result of various samples is presented in Figure 9. Better hardness is seen in the EC5 sample, probably due to more carbon than in other samples. This is alignment with the Merneedi et al. (2021) that investigate an increase in the coating hardness is caused by a growth in carbon content. Moreover, Haddadi et al. (2019) have found that presenting carbon in the epoxy composite coating could enhance the reinforcement of the soft polymeric material properties. Consequently, the increased carbon concentration in the coating contributed to increased hardness

3.7 Corrosion Test

The corrosion behavior of the various coated samples is measured by a three-cell electrode. A corrosion test in the 3.5% sodium chloride solution was conducted. An anodic scan was performed with a potential range between 0.5 to -0.2 V vs Ag/AgCl. The corrosion test measurement of various samples is presented in Figure 10. Corrosion potential (E_{corr}) can be found in Figure 10, while corrosion current density (I_{corr}) is found using the Tafel extrapolation method. After I_{corr} was found, CR could be calculated using Equation (2). E_{corr}, I_{corr}, and CR are summarized in Table 2.

Table 2. Corrosion Analysis Result

Coating	E_{corr} (V) vs Ag/AgCl	I_{corr} (A/cm^2)	CR (mmpy)
EC1	-1.138	7.468×10^{-7}	8.68×10^{-3}
EC3	-0.466	4.824×10^{-6}	5.61×10^{-2}
EC5	-1.168	4.856×10^{-7}	5.65×10^{-4}

Li et al. (2022) have found that CNDs content (0.05 wt.%, 0.15 wt.%, and 0.20 wt.%) in carbon/epoxy coating is independent of the porosity of the layer. Presenting 0.15 wt.% of CNDs in the epoxy could improve anti-corrosion due to the ability to fill up to 100% of the porosity of the coating film. On the contrary, Khun et al. (2014) in their study adding various MWCNT (0.1 wt.% and 0.5 wt.%), resulting in increased MWCNT lead to increase in corrosion resistance due to more MWCNT lead to increase pore resistance. Therefore, could be concluded that porosity of the coating is significant influence the corrosion resistance.

According to Lin and Lee, the SPCC plate has an I_{corr} 3.75×10^{-5} A/cm^2 in 3% NaCl (Lin and Lee, 2019). Coating SPCC plates using composite coating would decrease the I_{corr} (see Table 2). EC1 and EC5 have outstanding criteria, and EC3 has excellent standards, according to Shadravan et al. (2015). It seems corrosion resistance is dependent on the coating thickness. Shifting to thicker is promoted to reach better protection and result in more corrosion resistance. This behavior is probably due to more thickness promoted to decrease in porosity; therefore, better corrosion resistance is seen in the higher coating thickness (Farhadian et al., 2020).

Moreover, sample EC3 has E_{corr} -0.466 V vs Ag/AgCl, which indicates the coating has poor protection (lowest corrosion resistance) due to less thickness than the other samples, therefore the measured E_{corr} is the SPCC plate. This statement was corroborated to the others study (Lin et al., 2017; Lin and Lee, 2019). Lin et al. (2017) research show that SPCC has E_{corr} -0.467 to -0.604 V vs Ag/AgCl in 0.5% NaCl . Meanwhile, SPCC has E_{corr} -0.72 V vs Ag/AgCl in 3% NaCl (Lin and Lee, 2019).

4. CONCLUSION

Synthesis of the epoxy/carbon was successful according to the FTIR. An intensification in the highest intensity and a rise in the unevenness and surface roughness were affected by increases the carbon content. Increased surface roughness of the composite coating leads to increasing hydrophobicity. Hardness also increases by increasing the carbon content due to presenting carbon in the epoxy composite coating could enhance the coating physical properties. Coating thickness contributes to corrosion resistance, which means more coating thickness is better for the corrosion resistance of the coated sample. The layer thickness of 60.8 μm with 5 wt.% of carbon content would result in superior protection for SPCC plate due to its hardness and corrosion resistance.

5. ACKNOWLEDGMENT

BLU POK funding Engineering Faculty Universitas Negeri Jakarta with contract number 866/UN39/HK.02/2023, T/066 /5.FT/Kontrak-Penelitian/ PT.01.03/III/2023.

REFERENCES

Akafuah, N. K., S. Poozesh, A. Salaimeh, G. Patrick, K. Lawler, and K. Saito (2016). Evolution of the Automotive Body Coating Process—A Review. *Coatings*, **6**(2); 24

Al-Zu'bi, M., L. Anguilano, and M. Fan (2023). Effect of Incorporating Carbon- and Silicon-Based Nanomaterials on the Physico-Chemical Properties of a Structural Epoxy Adhesive. *Polymer Testing*, **128**; 108221

Almansoori, N., S. Aldulaijan, S. Althani, N. M. Hassan, M. Ndiaye, and M. Awad (2021). Manual Spray Painting Process Optimization Using Taguchi Robust Design. *International Journal of Quality and Reliability Management*, **38**(1); 46–67

Asemani, M. and A. R. Rabbani (2020). Detailed FTIR Spectroscopy Characterization of Crude Oil Extracted Asphaltenes: Curve Resolve of Overlapping Bands. *Journal of Petroleum Science and Engineering*, **185**; 106618

Basha, S. I., M. A. Aziz, S. Ahmad, M. M. Al-Zahrani, M. Shameem, and M. Maslehuddin (2022). Improvement of Concrete Durability Using Nanocomposite Coating Prepared by Mixing Epoxy Coating with Submicron/Nano-Carbon Obtained from Heavy Fuel Oil Ash. *Construction and Building Materials*, **325**; 126812

Bibi, S., S. Sarfaraz, M. Yar, M. I. Zaman, A. Niaz, A. Khan, and K. Ayub (2022). Structure And Electronic Characterization Of Pristine And Functionalized Single Wall Carbon

Nanotube Interacting With Sulfide Ion: A Density Functional Theory Approach. *Journal of Molecular Liquids*, **366**; 120144

Bouhamed, A., S. Choura, and O. Kanoun (2018). Impact Of Surface Modification Via Plasma Treatment On The Response Of Strain Sensor Based On MWCNTs/Epoxy Nanocomposite. In *2016 Nanotechnology for Instrumentation and Measurement (NANOfIM)*. pages 5–16

Chen, S., X. Wang, G. Zhu, Z. Lu, Y. Zhang, X. Zhao, and B. Hou (2021). Developing Multi-Wall Carbon Nanotubes/Fusion-Bonded Epoxy Powder Nanocomposite Coatings With Superior Anti-Corrosion And Mechanical Properties. *Colloids and Surfaces A: Physicochemical and Engineering Aspects*, **628**; 127309

Cheng, X., Q. Han, B. Yue, M. Shi, and C. Yang (2023). Self-Assembled Nano-Polymers Modified Water-Based Sizing Agent For Enhancing The Dual Interfacial Properties Of Carbon Fibre/Epoxy Resin Composites. *Composites Part B: Engineering*, **262**; 110828

Deyab, M. A., N. Hamdi, M. Lachkar, and B. E. Bali (2018). Clay/Phosphate/Epoxy Nanocomposites For Enhanced Coating Activity Towards Corrosion Resistance. *Progress in Organic Coatings*, **123**; 232–237

Duleba, B., F. Greskovic, L. Dulebová, and T. Jachowicz (2015). Possibility of increasing the mechanical strength of carbon/epoxy composites by addition of carbon nanotubes. *Materials Science Forum*, **818**; 299–302

Edvardsen, L., M. Grandcolas, S. Lædre, J. Yang, T. Lange, R. Bjørge, and K. Gawel (2021). Conductive Epoxy/carbon Nanofiber Coatings for Scale Control. *Surface and Coatings Technology*, **425**; 127694

Eskizeybek, V., A. Avcı, and A. Gülce (2017). Preparation and Mechanical Properties of Carbon Nanotube Grafted Glass Fabric/epoxy Multi-Scale Composites. *Advanced Composite Materials*, **26**(2); 169–180

Farhadian, M., K. Raeissi, M. Golozar, S. Labbaf, T. Hajilou, and A. Barnoush (2020). 3D-Focused Ion Beam Tomography and Quantitative Porosity Evaluation of ZrO_2-SiO_2 Composite Coating; Amorphous SiO_2 As a Porosity Tailoring Agent. *Applied Surface Science*, **511**; 145567

Freshtegan, A., M. Talaie, S. Aghamiri, and A. Khosropour (2016). Modifying Functionalized-Carbon-Nanotube Capacity to Enhance Water-Vapor Adsorption Capacity from Nitrogen Gas. *Gas Processing Journal*, **4**(2); 79–88

Haddadi, S., S. Ramazani, M. Mahdavian, P. Taheri, and J. Mol (2019). Mechanical and Corrosion Protection Properties of a Smart Composite Epoxy Coating with Dual-Encapsulated Epoxy/polyamine in Carbon Nanospheres. *Industrial & Engineering Chemistry Research*, **58**(8); 3033–3046

Hassan, H., L. Attia, and G. Dakroury (2020). Exploration of the Parameters Affecting the Radioactive Europium Removal from Aqueous Solutions by Activated Carbon-Epoxy Composite. *Applied Radiation and Isotopes*, **164**; 109278

Jin, F., X. Li, and S. Park (2015). Synthesis and Application of Epoxy Resins: A Review. *Journal of Industrial and Engineering Chemistry*, **29**; 1–11

Khun, N., B. Troconis, and G. Frankel (2014). Effects of Carbon Nanotube Content on Adhesion Strength and Wear and Corrosion Resistance of Epoxy Composite Coatings on AA2024-T3. *Progress in Organic Coatings*, **77**(1); 72–80

Knoll, J., B. Riecken, N. Kosmann, S. Chandrasekaran, K. Schulte, and B. Fiedler (2014). The Effect of Carbon Nanoparticles on the Fatigue Performance of Carbon Fibre Reinforced Epoxy. *Composites Part A: Applied Science and Manufacturing*, **67**; 233–240

Kurniawan, O. and B. Soegijono (2020). Preparation and Characterization of Polyurethane/Carbon/Organoclay Composite for Coating of Aluminum Conductor Overhead Lines. *E-Journal of Surface Science and Nanotechnology*, **18**; 62–69

Li, S., F. Du, Y. Lin, Y. Guan, W. J. Qu, J. Cheng, and D. Wang (2022). Excellent Anti-Corrosion Performance of Epoxy Composite Coatings Filled with Novel N-Doped Carbon Nanodots. *European Polymer Journal*, **163**; 110957

Liang, W. J., B. Zhao, C. Y. Zhang, R. K. Jian, D. Y. Liu, and Y. Q. Liu (2017). Enhanced Flame Retardancy of DGEBA Epoxy Resin with a Novel Bisphenol-A Bridged Cyclotriphosphazene. *Polymer Degradation and Stability*, **144**; 292–303

Lin, C. H. and J. R. Lee (2019). Characterization of SPCC Steel Stress Behaviour in Brine Water Environment. *International Journal of Electrochemical Science*, **14**(3); 2321–2332

Lin, C. H., J. R. Lee, H. H. Sheu, and S. Y. Tsai (2017). Corrosion Resistance and Mechanical Property Enhancement of SPCC Steel Using an Induction Heat Treatment. *International Journal of Electrochemical Science*, **12**(9); 7965–7976

Luangkularb, S., S. Prombanpong, and V. Tangwarodomnukun (2014). Material Consumption and Dry Film Thickness in Spray Coating Process. *Procedia CIRP*, **17**; 789–794

Ma, Z., B. Ouyang, and X. Zuo (2024). Study on Plasma Modified Silica Powder Epoxy Resin Composites. *Journal of Adhesion Science and Technology*; 1–19

Maron, G. K., B. S. Noremberg, J. H. Alano, F. R. Pereira, V. G. Deon, R. C. R. Santos, and N. L. V. Carreno (2018). Carbon Fiber/Epoxy Composites: Effect of Zinc Sulphide Coated Carbon Nanotube on Thermal and Mechanical Properties. *Polymer Bulletin*, **75**(4); 1619–1633

Mateab, S. H. and M. Albozahid (2022). Study the Effect of Adding MWCNTs on the Hardness, Impact Strength, and Structural Properties of Composite Materials Based on Epoxy Polymer. *Egyptian Journal of Chemistry*, **65**(3); 147–152

Merneedi, A., L. Natrayan, S. Kaliappan, D. Veeman, S. Angalaeswari, C. Srinivas, and P. Paramasivam (2021). Experimental Investigation on Mechanical Properties of Carbon Nanotube-Reinforced Epoxy Composites for Automobile Application. *Journal of Nanomaterials*, **2021**(1); 4937059

Mora, A. S., R. Tayouo, B. Boutevin, G. David, and S. Caillol (2020). A Perspective Approach on the Amine Reactivity and the Hydrogen Bonds Effect on Epoxy-Amine Systems. *European Polymer Journal*, **123**; 109460

Netkueakul, W., D. Korejwo, T. Hammer, S. Chortarea, P. Rupper, O. Braun, and J. Wang (2020). Release of Graphene-Related Materials from Epoxy-Based Composites: Characterization, Quantification and Hazard Assessment: In Vitro. *Nanoscale*, **12**(19); 10703–10722

Qi, Z., Y. Tan, H. Wang, T. Xu, L. Wang, and C. Xiao (2017). Effects of Noncovalently Functionalized Multiwalled Carbon Nanotube with Hyperbranched Polyesters on Mechanical Properties of Epoxy Composites. *Polymer Testing*, **64**; 38–47

Qu, C. B., Y. Huang, F. Li, H. M. Xiao, Y. Liu, Q. P. Feng, and S. Y. Fu (2020). Enhanced Cryogenic Mechanical Properties of Carbon Fiber Reinforced Epoxy Composites by Introducing Graphene Oxide. *Composites Communications*, **22**; 100480

Rwawiire, S., A. Kasedde, I. Nibikora, and G. Wandera (2014). Prediction of Polyester/Cotton Ring Spun Yarn Unevenness Using Adaptive Neuro Fuzzy Inference System. *Journal of Textile and Apparel, Technology and Management*, **8**(4); 1–12

Sakib, M. N. and A. A. Iqbal (2021). Epoxy Based Nanocomposite Material for Automotive Application - A Short Review. *International Journal of Automotive and Mechanical Engineering*, **18**(3); 9127–9140

Salam, H., Y. Dong, I. J. Davies, and A. Pramanik (2016). The Effects of Material Formulation and Manufacturing Process on Mechanical and Thermal Properties of Epoxy/Clay Nanocomposites. *International Journal of Advanced Manufacturing Technology*, **87**(5–8); 1999–2012

Shadravan, A., B. Hughes, M. Ghasemi, and M. Alfi (2015). Zonal Isolation in Geothermal Wells. *Fortieth Workshop on Geothermal Reservoir Engineering*, **January**; 25–26

Sheth, D., S. Maiti, S. Patel, J. Kandasamy, M. R. Chandan, and A. Rahaman (2020). Enhancement of Mechanical Properties of Carbon Fiber Reinforced Epoxy Matrix Laminated Composites with Multiwalled Carbon Nanotubes. *Fullerenes Nanotubes and Carbon Nanostructures*, **29**(4); 288–294

Soares-Pozzi, A. C. and D. Dibbern-Brunelli (2016). Study of the Influence of Saline Solutions in Carbon/Epoxy Composite by Luminescence, Raman and UATR/FT-IR Spectroscopy. *Journal of Materials Science*, **51**(20); 9342–9355

Sudha, G. S., H. Kalita, S. Mohanty, and S. K. Nayak (2017). Biobased Epoxy/Carbon Fiber Composites: Effect on Mechanical, Thermo-Mechanical and Morphological Properties. *Journal of Macromolecular Science, Part A: Pure and Applied Chemistry*, **54**(10); 756–764

Susetyo, F. B., B. Soegijono, and Yusmaniar (2021). Effect of a Constant Magnet Position and Intensity on a Copper Layer Obtained by DC Electrodeposition. *International Journal of Corrosion and Scale Inhibition*, **10**(2); 766–782

Vaßen, R., C. Made, E. Bakan, C. Gatzen, S. Kim, D. E. Mack, and O. Guillon (2019). Environmental Barrier Coatings Made by Different Thermal Spray Technologies. *Coatings*, **9**(12); 784

Wang, P. N., T. H. Hsieh, C. L. Chiang, and M. Y. Shen (2015). Synergetic Effects of Mechanical Properties on Graphene Nanoplatelet and Multiwalled Carbon Nanotube Hybrids Reinforced Epoxy/Carbon Fiber Composites. *Journal of Nanomaterials*; 1–9

Weng, M., Z. X. Huang, Q. W. Yuan, Z. H. Liu, and J. P. Qu (2024). Ultrawide Sensing-Range, Super Durable and High-Strength Epoxy/Carbon Fiber Composites Sensor Based on Stress-Induced Structure. *Composites Science and Technology*, **250**; 110522

Xia, Z., L. Shuan, and H. Baorong (2014). A Comparative Study of Neat Epoxy Coating and Nano ZrO2/Epoxy Coating for Corrosion Protection on Carbon Steel. *Applied Mechanics and Materials*, **599–601**; 3–6

Xu, Y., X. Sun, R. Shen, Z. Wang, and Q. Wang (2020). Thermal Behavior and Smoke Characteristics of Glass/Epoxy Laminate and Its Foam Core Sandwich Composite. *Journal of Thermal Analysis and Calorimetry*, **141**(3); 1173–1182

Zhang, L., W. Zhang, Y. Peng, W. Wang, and J. Cao (2022). Thermal Behavior and Flame Retardancy of Poplar Wood Impregnated with Furfuryl Alcohol Catalyzed by Boron/Phosphorus Compound System. *Industrial Crops and Products*, **176**; 114361

Zuo, Y., Z. Yao, H. Lin, J. Zhou, X. Guo, and H. Cai (2019). Synthesis and Characterization of Carbonyl Iron@Epoxy Core–Shell Microspheres for Enhanced Microwave Absorption Performance. *Journal of Materials Science*, **54**(18); 11827–11840

